Climate Data Record (CDR) Program

Technical Note for IASI/CrIS Data Extension for Outgoing Longwave Radiation (OLR) – Monthly

CDR Program Document Number: CDRP-RPT-1443
Configuration Item Number: 01B-06
Revision 0 / Nov 13, 2023
DSR Number: DSR-1841

REVISION HISTORY

Rev.	Author	DSR No.	Description	Date
0	Hai-Tien Lee Univ. of Maryland	DSR-1841	Technical Note for IASI/CrIS data extension for OLR-Daily 2007 - current	11/01/2023

TABLE of CONTENTS

LIST of FIGURES

LIST of TABLES

Introduction

1.1 Purpose

The objective of this document is to furnish details about the updated Monthly Outgoing Longwave Radiation (OLR) Climate Data Record (CDR) dataset, version v02r07, spanning from 2007 to the present, featuring an extension incorporating IASI/CrIS data.

For the current operational v02r07 Monthly OLR CDR, refer C-ATBD by Lee (2017).

This release serves as an interim measure to guarantee the accessibility and uninterrupted continuity of the OLR CDR dataset, given the imminent possibility of decommissioning of HIRS instruments. In light of its provisional nature to address the present circumstances, the version number and file names remain unchanged, with modifications limited to metadata updates.

The internal designation for the extended IASI/CrIS data from 2007 to the present will be referred to as "v2.8" henceforth, whereas the previous v02r07 operational product will be labeled as "v2.7" to ensure clear distinction.

Previously the OLR CDR relied primarily on HIRS OLR retrievals. Recent years we have discovered artifacts in trends and uncertainties due to deteriorating HIRS instruments and the unfavorable orbital drift towards evening hours. The inclusion of IASI/CrIS OLR retrievals not only enhances the accuracy of OLR retrievals but also complements diurnal sampling. This effectively mitigates trend artifacts and significantly improves overall accuracy.

The forthcoming significant upgrade, set for release in June 2025 as Monthly OLR CDR v03r00, will encompass a comprehensive reprocessing of the entire Monthly OLR CDR dataset dating back to 1979. This initiative is aimed at effectively addressing and rectifying the issues that have been identified and persisted throughout the years.

1.2 Referencing this Document

This document should be referenced as follows:

Technical Note for IASI/CrIS Data Extension for OLR-Monthly CDR.

1.3 Products Relevant to this Document

Table 1 describes the versions of the Monthly OLR CDR product releases with their corresponding software package and the CATBD versions.

Table 1 Version tracking for the MONTHLY OLR CDR product releases.

Product Version	Software Version	CATBD Revision	Release Date	Remarks
v02r07	v02r07	v1	2014-06-10	Initial Release
v02r07	v02r07	Technical Note for IASI/CrIS Data Extension 2007-present for Monthly OLR CDR	2023-11-01	Intermediate release. Version unchanged. See Technical note.
v03r00	v03r00	v2	2025-06-30	Major update

IASI and CrIS OLR Retrievals

2.1 IASI and CrIS OLR Algorithms

The hyperspectral OLR estimation principles and IASI OLR retrieval algorithm are explained here.

The total outgoing longwave radiative flux density, OLR, is the integral of the spectral fluxes over the thermal radiation spectrum,

$$\mathrm{OLR} = \int \mathrm{F}_\nu \mathrm{d}\nu \qquad (1)$$

The spectral flux F_ν *at frequency* ν is the integral of the normal specific radiances at the top of the atmosphere z_t, over the hemispheric dome related to the local zenith angle θ and azimuthal angle ϕ,

$$\mathrm{F}_\nu = \int_0^{2\pi} \int_0^{\pi/2} \mathrm{I}_\nu(z_t;\, \theta, \phi) \cos\theta \sin\theta \, \mathrm{d}\theta \, \mathrm{d}\phi \qquad (2)$$

Frequency-dependent Spectral Angular Models (SAM), can be constructed to approximate the spectral flux integral, for a radiance observation at local zenith angle θ, such that,

$$\mathrm{F}_\nu \cong \mathrm{SAM}_\nu(\mathrm{I}_\nu(z_t;\, \theta)) \qquad (3)$$

There are two principles that make the spectral flux estimation possible with the spectral angular models:

1. ***Inter-Frequency Correlations*** - *Radiances at one frequency are strongly correlate with radiances at another with similar absorption features.*
2. ***Intra-Frequency/Angle Correlations*** - *Using "absorption strength" as surrogate to "optical path length", spectral flux integration can be estimated with radiances at selected angles (as in Gaussian quadrature)*

Previous works can be found in Lee, Ellingson & Gruber (2010); Turner, Lee & Tett (2015).

The IASI OLR algorithm is a 3-predictor multiple linear regression model in quadratic forms, whereas the predictors are natural log of IASI radiances aggregated to 10 cm^{-1} intervals in 650-2500 cm^{-1} range. Note that the IASI radiance observations over 2500-2760 cm^{-1} are not used due to possible solar contamination.

$$\begin{aligned} log(F_\nu) = {} & a_0(\nu,\theta) + a_1(\nu,\theta)\, x_1(\nu,\theta) + a_2(\nu,\theta)\, x_2(\nu,\theta) + \\ & a_3(\nu,\theta)\, x_3(\nu,\theta) + a_4(\nu,\theta)\, \mathrm{x}_1^2(\nu,\theta) + \\ & a_5(\nu,\theta)\, \mathrm{x}_2^2(\nu,\theta) + a_6(\nu,\theta)\, \mathrm{x}_3^2(\nu,\theta) \end{aligned} \qquad (4)$$

where,

$$x_\nu = \log(I_\nu(\theta)) \quad (5)$$

with the frequency and zenith angle-dependent regression coefficients a's.

Figure 1 shows the correlations between the spectral flux and radiance at different zenith angles. The strongest correlations can be seen near 53° and this is related to the diffusivity approximation. The spectral locations with strong absorption features tend to produce weaker correlations for zenith angles outside vicinity of 53°, and this is where the Intra-frequency/angle correlations become useful for the spectral flux estimation.

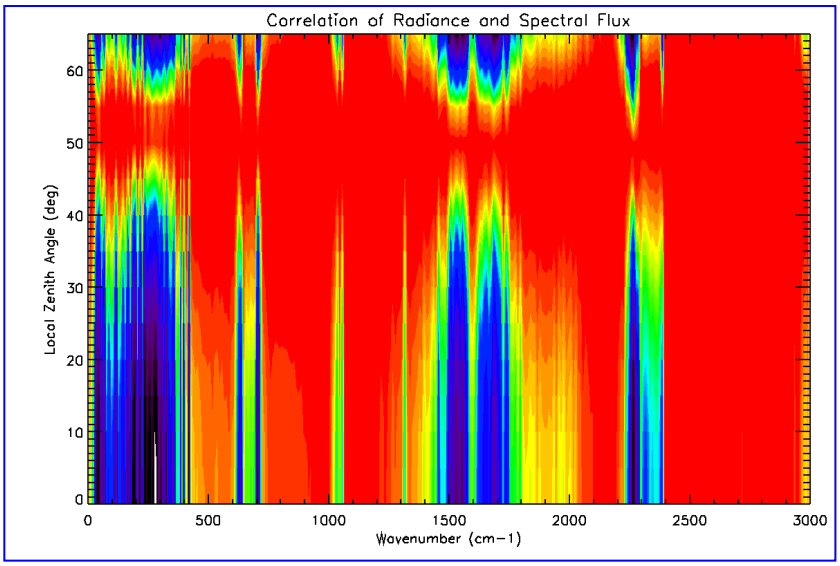

Fig. 1 Correlation between spectral fluxes and radiances at different local zenith angles.

Figure 2 shows the selection of the predicting radiances for the estimation of spectral fluxes at each 10 cm^{-1} wavenumber band. The estimate of the IASI OLR estimation errors are shown in **Figure 3**, where the rms total estimation errors range from 0.13 - 0.47 Wm^{-2}. The far infrared (FIR) spectral domain, 0-650 cm^{-1} contributed the most of the errors, due that the FIR spectrum are not directly observed and the spectral fluxes are not well correlated to radiance observations at most of the angles.

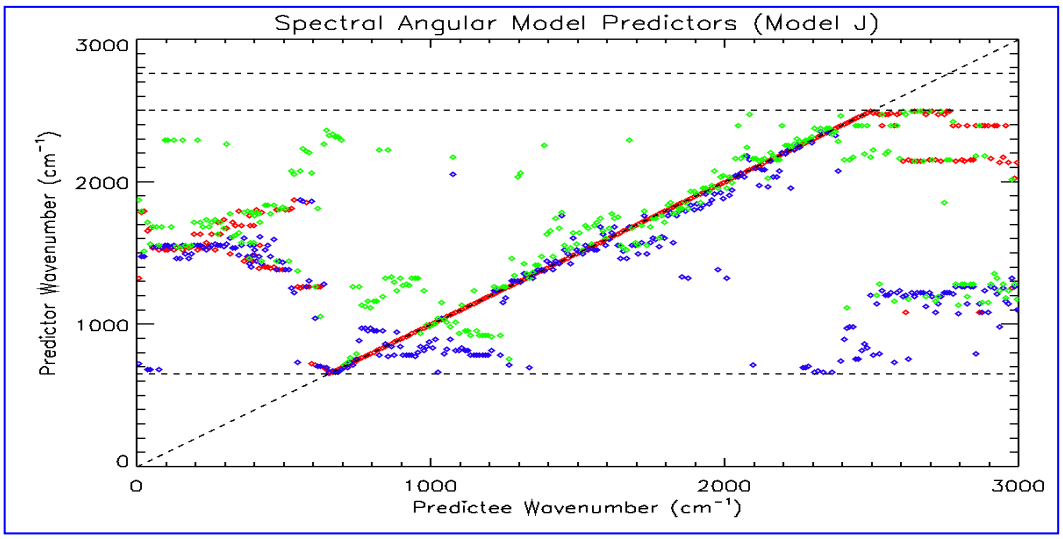

Fig. 2 Selections of predicting radiances (y-axis) for the estimation of spectral fluxes (x-axis) at each 10 cm-1 wavenumber band, with IASI radiance observations in 650-2500 cm-1 range. There are three selected predicting radiances wavenumbers at each spectral band, represented by colors red, blue and green.

.

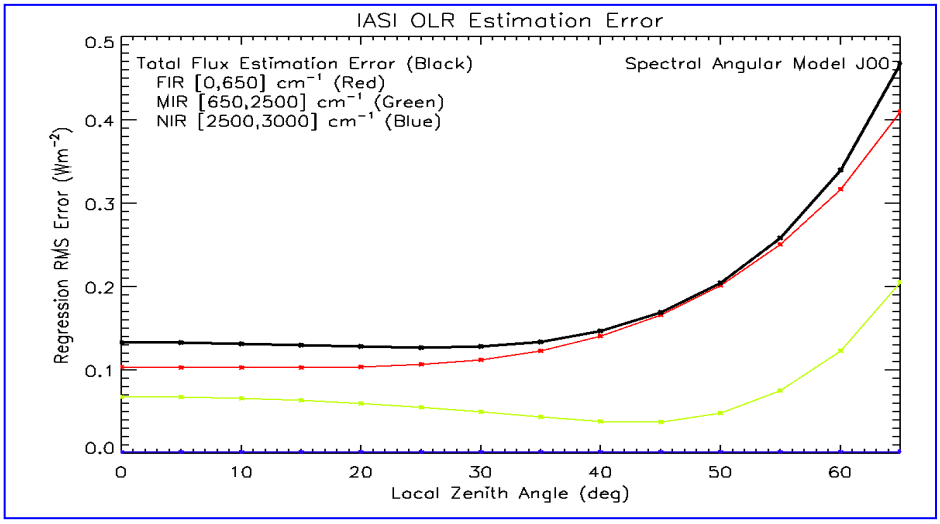

Fig. 3 RMS regression errors for the total OLR estimation, as a function of the observing local zenith angle, range from 0.13 - 0.47 Wm-2, and are dominated by flux estimation errors from the “FIR” spectral domain.

Note that the CrIS OLR algorithm shares the similar estimation principle and model design, except some part of the mid thermal spectrum not directly observed by CrIS would have to be estimated from the observed CrIS radiances.

2.2 Data availability

Table 2 provide the data temporal coverage of operational products of IASI and CrIS observations. **Figure 4** shows the observation local time for the HIRS, IASI and CrIS data onboard of the respective TIROS-N, Metop and JPSS-series satellites.

Table 2 Data availability of IASI and CrIS observations.

Satellite / Instrument	Data Type	Period of Observations
M02/Metop-A IASI	Level 1C	2007-05-21 to 2021-10-15
M01/Metop-B IASI	Level 1C	2013-08-01 to present
M03/Metop-C IASI	Level 1C	2019-07-06 to present
Suomi-NPP CrIS	NSR SDS (prior to 2017-03-08); FSR SDS	2012-04-19 to 2021-05-21 (Degraded since 2021.05.21 without OLR retrievals)
NOAA20/JPSS-01 CrIS	FSR SDS	2017-03-08 to present (with significant missing in 2021.05)
NOAA21/JPSS-02 CrIS	FSR SDS	2023-04-12 to present

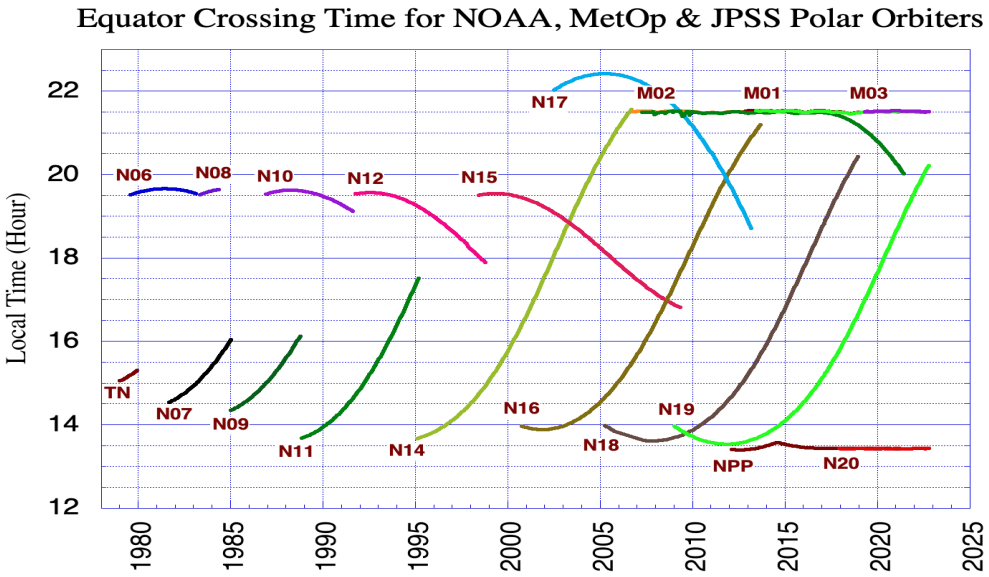

Fig. 4 Equator crossing times for the ascending orbit of the NOAA POES TIROS-N, Metop and JPSS-series satellites.

Inter-satellite Calibration

3.1 Calibrate M02 IASI against M02 HIRS

The intermediate upgrade of the Monthly OLR CDR v2.8 is meant to ensure the continued data availability and continuity of the current operational Monthly OLR CDR v02r07. The newly added IASI and CrIS OLR retrievals are thus calibrated to the absolute radiometric standard of the v02r07 Monthly OLR CDR, that is the HIRS OLR from NOAA-9.

The HIRS OLR and IASI/CrIS regression models are determined with simulated radiation radiances and fluxes databases with similar configurations. However, due to the significant differences in the instruments and the OLR retrieval algorithms, the OLR retrievals are showing some discrepancies. The inter-satellite calibration serves the purpose to eliminated the global and regional differences between the HIRS-retrieved OLR and the IASI/CrIS-retrieved OLR.

The inter-satellite calibration between the M02-HIRS and M02-IASI is the primary tool to maintain the continuity of the OLR CDR.

The method adopted to calibrate M02-IASI to M02-HIRS is the zonal adjustments with linear equations that is dependent on the IASI OLR. We found that the global bias adjustment or theme-dependent bias adjustment are insufficient to produce acceptable agreement between the two retrievals.

The zonal adjustments calibration equations were determined by the data from the respective OLR monthly ascending and descending 2.5° gridded maps, over the common period of 2007.01 – 2016.11. (HIRS data post 2016.12 started to show significant increase of noises.)

For the M02 IASI OLR retrievals within the latitude band φ_i, the adjusted M02 IASI OLR is obtained through the linear adjustment

$$OLR_{M02IASI}^{Adjusted}(\varphi_i) = a_0(\varphi_i) + a_1(\varphi_i)\, OLR_{M02IASI}(\varphi_i) \qquad (6)$$

where φ_i is the 2.5° latitudinal band and a's are the regression coefficients for the corresponding latitudinal band.

Figure 5 shows sample comparisons for the biases between M02 IASI and M02 HIRS, before and after the inter-satellite adjustment, where significant improvements can be seen over the ITCZ and other convective cloud zones.

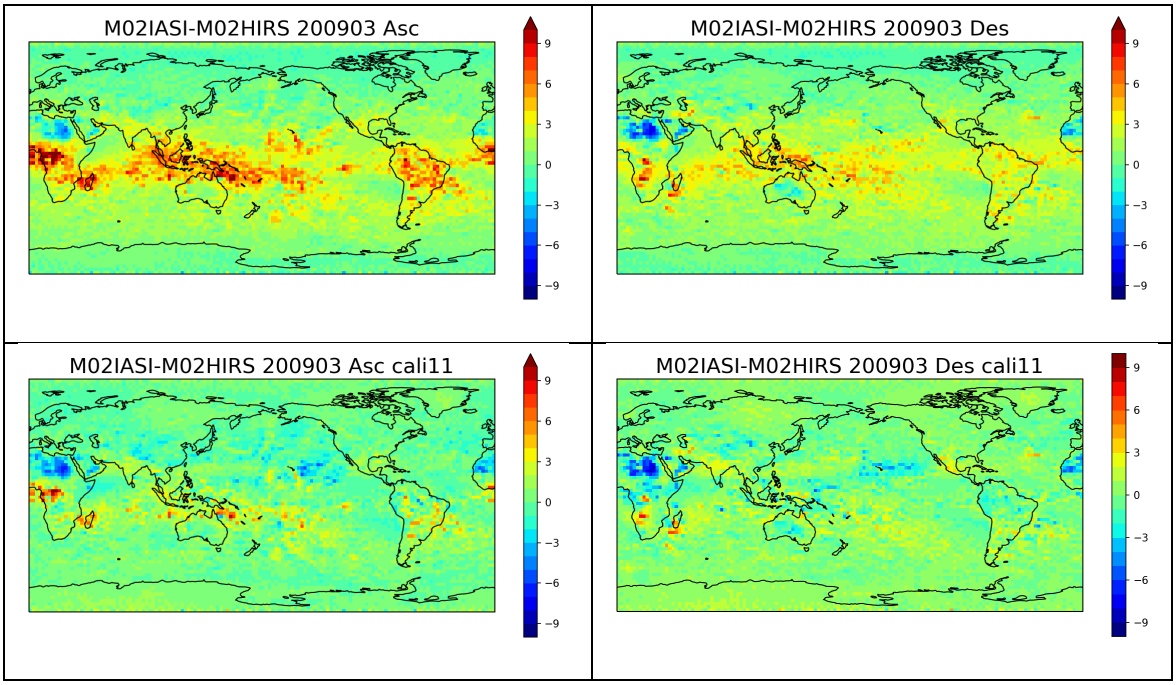

Fig. 5 Monthly mean nodal maps of OLR differences between M02-IASI and M02-HIRS for March 2009 before (top row) and after (bottom row) the application of the zonal intersatellite calibration adjustment.

3.2 Calibrate remaining IASI/CrIS against M02 IASI

For the OLR retrievals from M01, M03 IASI and NPP, J01 and J03 CrIS, they are adjusted by a global bias relative to M02-IASI, determined with the field-of-view (FOV) collocated OLR retrievals over long overlapping time.

Changes from Monthly OLR CDR v2.7 to v2.8

The changes in Monthly OLR CDR from v2.7 to v2.8 are shown in this section, and the v2.8 is making improvements in most cases. The CERES EBAF Ed4.2and EBAF Ed4.2 OLR products are used for the performance assessment.

4.1 Evaluation with CERES EBAF data

The Monthly OLR CDR v2.7 (aka, the current operational product v02r07) and the newly constructed v2.8 with IASI and CrIS OLR are compared to the CERES EBAF Ed4.2OLR product.

Figure 6 shows the average OLR differences for v2.7 and v2.8 Monthly OLR CDR, relative to the CERES EBAF Ed4.2 OLR product, over 2000.03-2022.12 period. The reduction of biases in v2.8 can be found in sub-tropics and over Sahara and Arabian deserts.

Figure 7 shows the standard deviation of the OLR differences for v2.7 and v2.8 Monthly OLR CDR, relative to CERES EBAF Ed4.2 OLR product. Clear reduction of random errors in v2.8 can be found in mid latitudes, western pacific warm pool and south east Asia – attributed to both better temporal sampling provided with the additional IASI and CrIS observations, particularly with the CrIS observations from the afternoon orbits, and higher accuracy of hyperspectral IASI and CrIS OLR retrievals.

Figure 8 shows the RMS OLR differences for v2.7 and v2.8 Monthly OLR CDR, relative to CERES EBAF Ed4.2 OLR product. The RMS OLR differences represent the overall accuracy performance of the Monthly OLR CDR, assessed with CERES EBAF Ed4.2 product, that the RMS OLR differences are lesser than 3 Wm^{-2} in most areas.

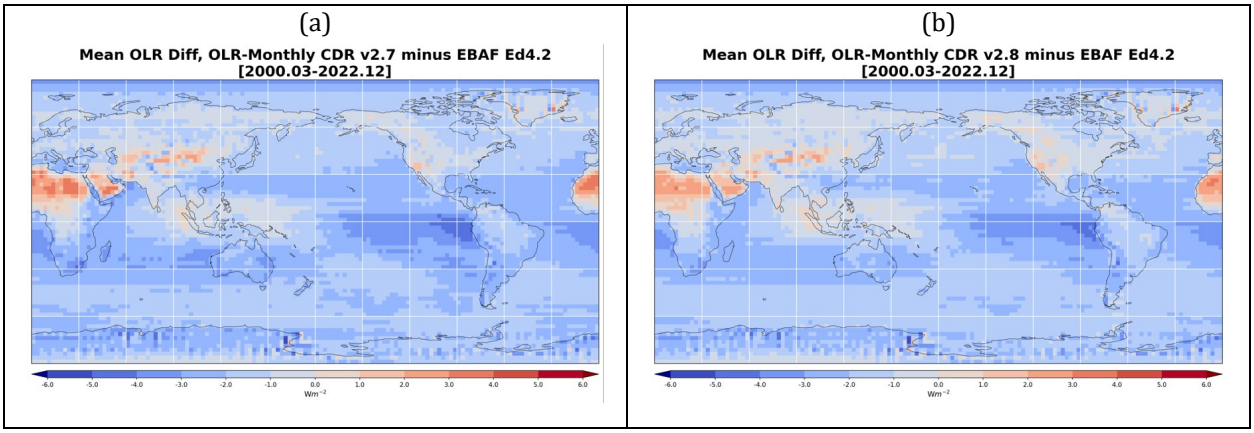

Fig. 6 Mean OLR differences for (a) v2.7 and (b) v2.8 Monthly OLR CDR, relative to CERES EBAF Ed4.2 OLR product, over 2000.03-2022.12 period.

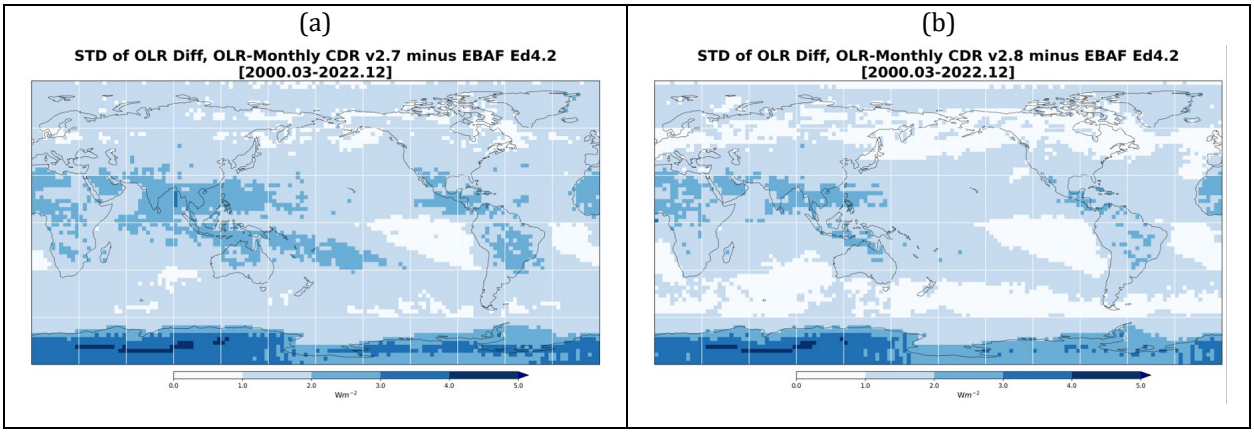

Fig. 7 Standard Deviation of OLR differences for (a) v2.7 and (b) v2.8 Monthly OLR CDR, relative to CERES EBAF Ed4.2 OLR product, over 2000.03-2022.12 period.

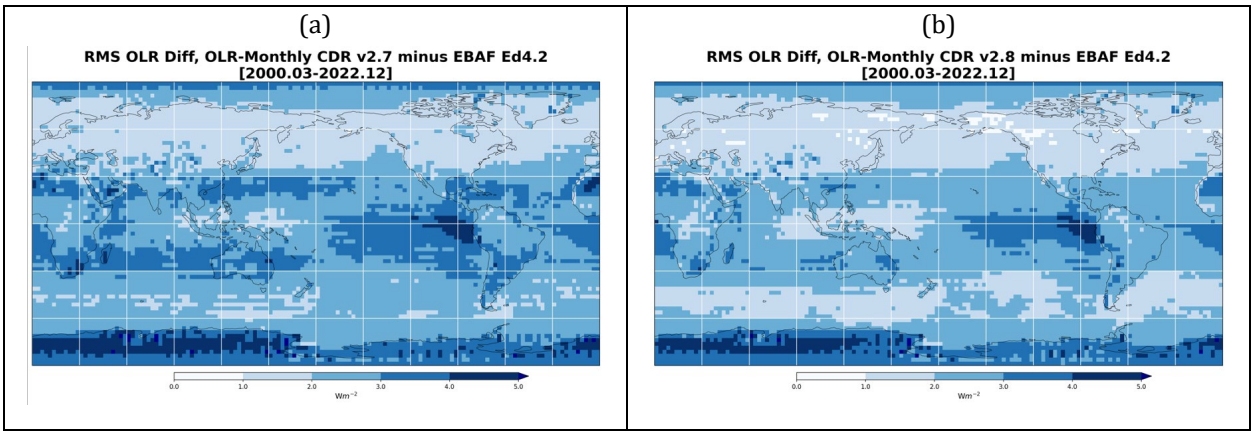

Fig. 8 RMS OLR differences for (a) v2.7 and (b) v2.8 Monthly OLR CDR, relative to CERES EBAF Ed4.2 OLR product, over 2000.03-2022.12 period.

Figures 9 and 10 show the time series of the mean, standard deviation, and rms OLR differences for Monthly OLR CDR v2.7 and v2.8, relative to the CERES EBAF Ed4.2product, for global and tropical domain average, respectively. The notable changes are in the mean and standard deviation of the OLR differences. The gradual increases (negatively) of the OLR differences between v2.7 and EBAF after 2016 have been removed in v2.8. This is likely be attributed to the added diurnal sampling time with the IASI and CrIS observations. The standard deviation of OLR differences in v2.8 are now more stable, eliminating the increase after 2016 seen in v2.7. This can be attributed to the better OLR retrievals from IASI and CrIS and the removal of some bad/noisy HIRS OLR retrievals through QC.

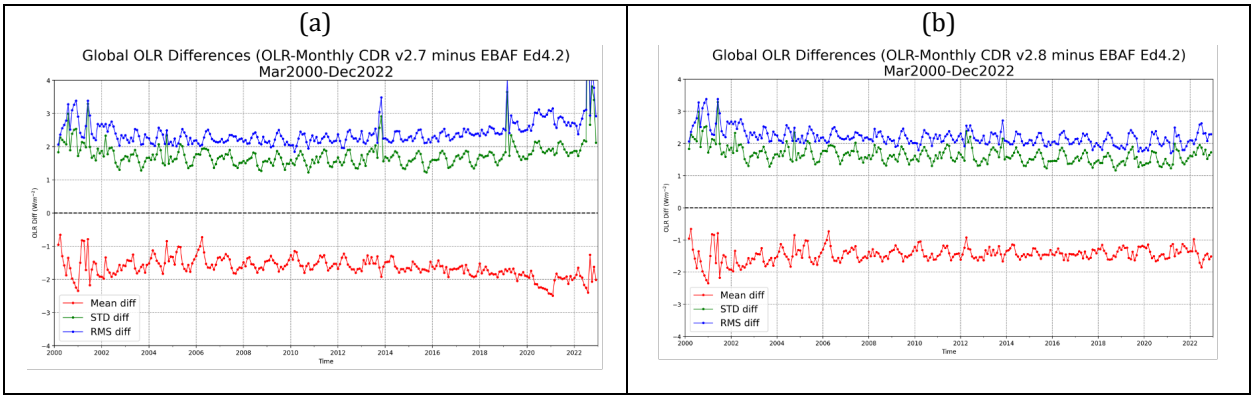

Fig. 9 Global mean OLR differences for (a) v2.7 and (b) v2.8 Monthly OLR CDR, relative to CERES EBAF Ed4.2OLR product, over 2000.03-2022.12 period.

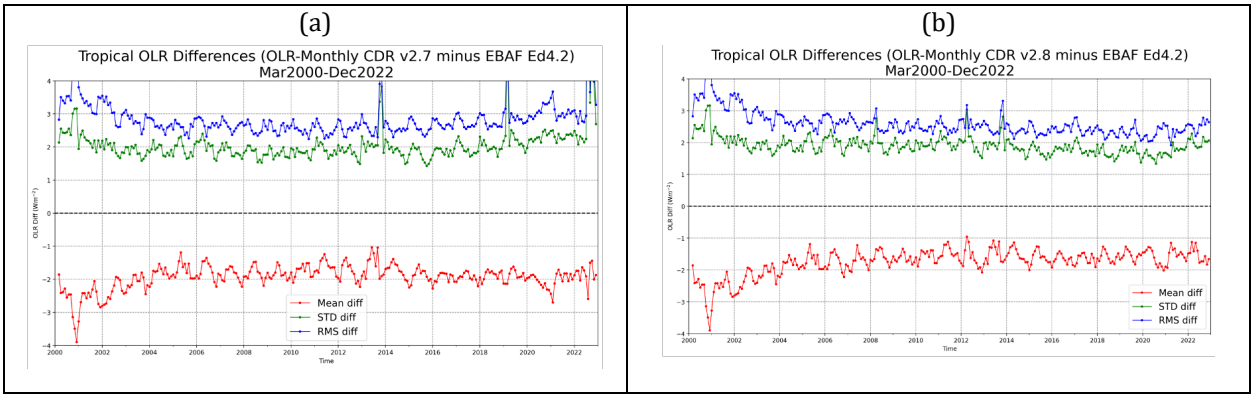

Fig. 10 Tropical 20S-20N mean OLR differences for (a) v2.7 and (b) v2.8 Monthly OLR CDR, relative to CERES EBAF Ed4.2OLR product, over 2000.03-2022.12 period.

Figures 11 and 12 show the time series of the OLR anomalies from Monthly OLR CDR v2.7 and v2.8, and the CERES EBAF Ed4.2 product, for global and tropical domains, respectively. The Monthly OLR CDR v2.8 OLR anomalies track accurately with those from the EBAF Ed4.2 product, eliminating the apparent departures in v2.7 after 2018.

Figures 13 and 14 show the time series of the mean differences of the OLR anomalies for Monthly OLR CDR v2.7 and v2.8, relative to the CERES EBAF Ed4.2 product, for global and tropical domains, respectively. The negative departures of the OLR anomalies in v2.7 vs EBAF after 2016 no longer present in the v2.8.

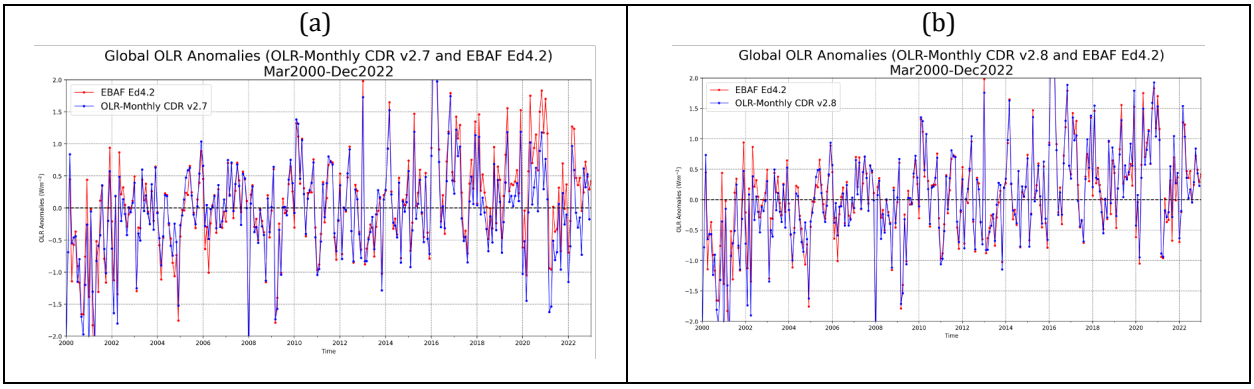

Fig. 11 Differences of global OLR anomalies for (a) v1.2 and (b) v1.3 Daily OLR CDR, relative to CERES EBAF Ed4.2 OLR product, over 2000.03-2022.12 period.

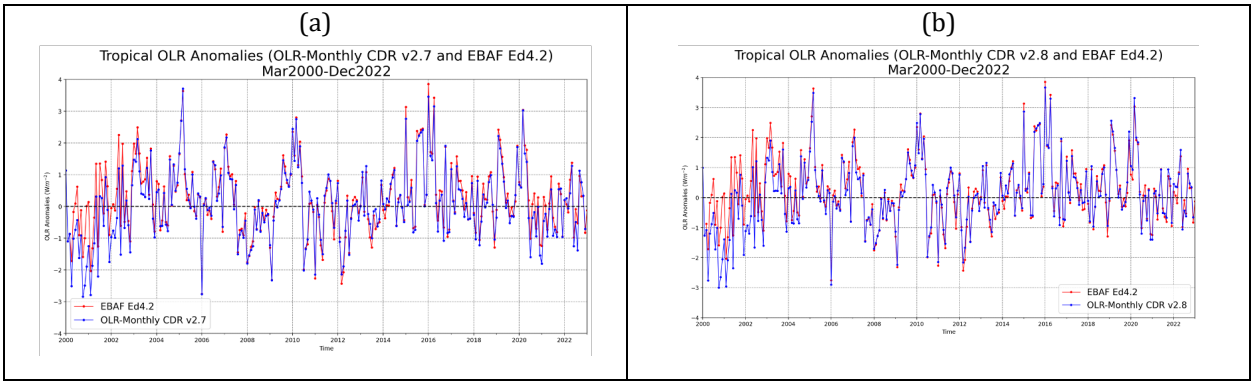

Fig. 12 Differences of tropical OLR anomalies for (a) v1.2 and (b) v1.3 Daily OLR CDR, relative to CERES EBAF Ed4.2 OLR product, over 2000.03-2022.12 period.

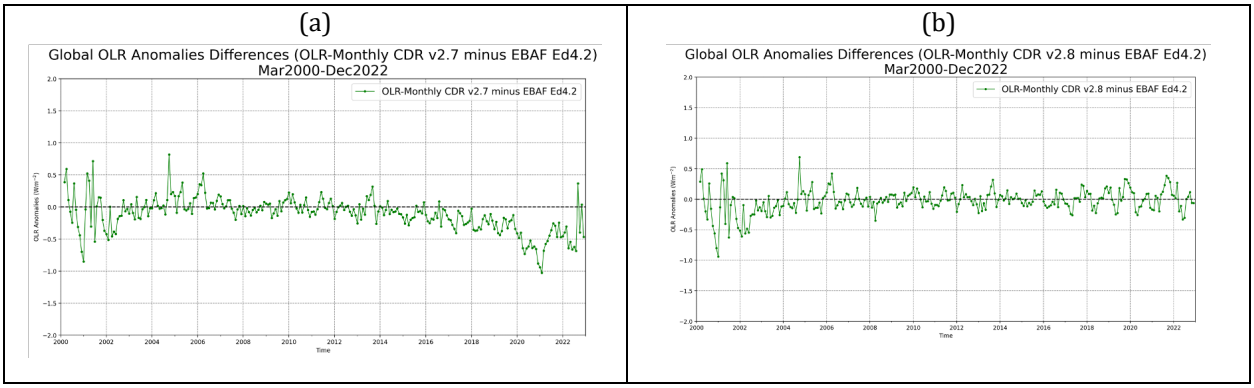

Fig. 13 Differences of global OLR anomalies for (a) v2.7 and (b) v2.8 Monthly OLR CDR, relative to CERES EBAF Ed4.2OLR product, over 2000.03-2022.12 period.

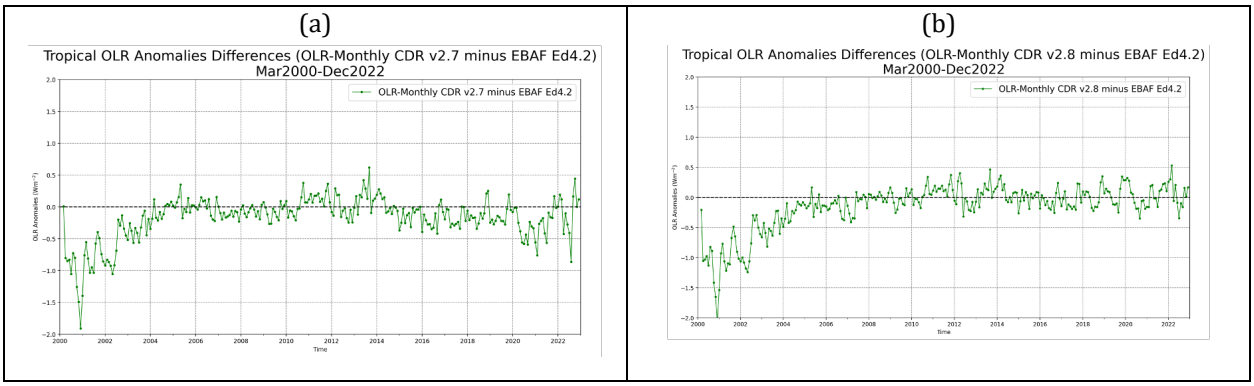

Fig. 14 Differences of tropical OLR anomalies for (a) v2.7 and (b) v2.8 Monthly OLR CDR, relative to CERES EBAF Ed4.2OLR product, over 2000.03-2022.12 period.

Table 3 summarize the statistics of the Monthly OLR CDR performances, in reference to the CERES EBAF Ed4.2product. The most significant changes are in the trend in the anomaly differences. The global anomalies in Monthly OLR CDR v2.7 has a -0.208±0.042 Wm-2/decade trend, relative to EBAF Ed4.2, and this is greatly improved to **-0.076±0.035 Wm-2/decade for v2.8.** Another set of assessment limits the comparison to the period after 2004.01 to avoid the single Terra satellite time and the early time with fast SW-degradation in SW and shortwave part of Total channels. The global anomalies in Monthly OLR CDR v2.8 relative to EBAF Ed4.2 has attained a stability of **-0.007±0.035 Wm-2/decade for v2.8.**

The overall accuracy assessment is represented by the global RMS OLR differences and it is **2.21 Wm-2** for the v2.8 Monthly OLR CDR, assessed with EBAF Ed4.2 product, and this is within the uncertainties of the EBAF OLR product, which is at about 1.5%.

Table 3 Summary statistics for the evaluation of Monthly OLR CDR v2.7 and v2.8, in reference to CERES EBAF Ed4.2product, over 2000.03-2022.12 period.

	CDRv2.7 – EBAF4.2	CDRv2.8 – EBAF4.2	Period
Global Mean diff	-1.63	**-1.44**	[2000.03-2022.12]
Global Std diff	1.77	**1.66**	
Global RMS diff	2.43	**2.21**	
Tropical Mean diff	-1.92	-1.74	
Tropical Std diff	2.07	1.92	
Tropical RMS diff	2.85	2.61	
Slope of Global Anom diff	-0.208 ± 0.042	**0.076 ± 0.035**	[2000.03-2022.12]
	-0.338 ± 0.042	**0.007 ± 0.035**	[2004.01-2022.12]
Slope of Tropical Anom diff	0.165 ± 0.058	**0.369 ± 0.054**	[2000.03-2022.12]
	-0.113 ± 0.047	**0.102 ± 0.041**	[2004.01-2022.12]
Corr of Global Anom	0.941	0.968	[2000.03-2022.12]
	0.942	0.982	[2004.01-2022.12]
Corr of Tropical Anom	0.956	0.944	[2000.03-2022.12]
	0.983	0.987	[2004.01-2022.12]

4.2 Changes in EBAF Ed4.2 from Ed4.1

The global mean differences of EBAF Ed4.2 and Ed4.1 OLR products are shown in **Figures 15.** Beside the global decrease of 0.1 Wm-2 from Ed4.1 to Ed4.2, there are also some reprocessing that modified the Ed4.1 data before 2003 and a month in 2004. The reprocessing of pre-2003 EBAF data lead to better agreement between Monthly OLR CDR and EBAF. **Figure 16** shows the improved agreement in Monthly OLR CDR and the EBAF with the reprocessed EBAF Ed4.2 data in 2000-2002 period.

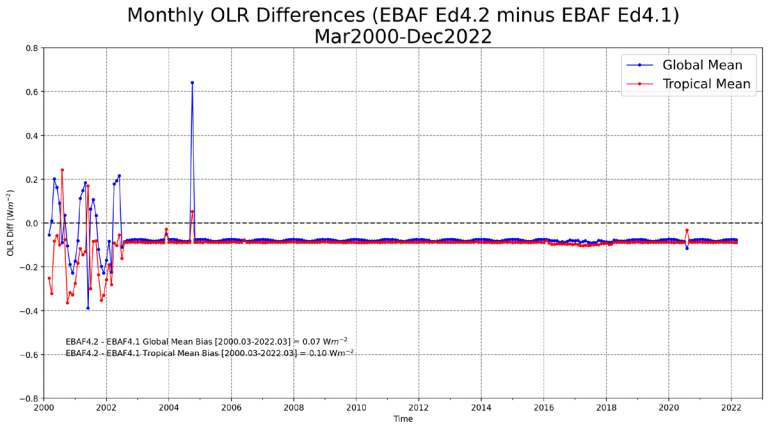

Fig. 15 Global mean OLR differences for v2.7 and v2.8 Monthly OLR CDR, relative to CERES EBAF Ed4.2OLR product. It shows improved stability (see green curve) and reduced random noises (red curve) in v2.8 Monthly OLR CDR, particularly after 2014.

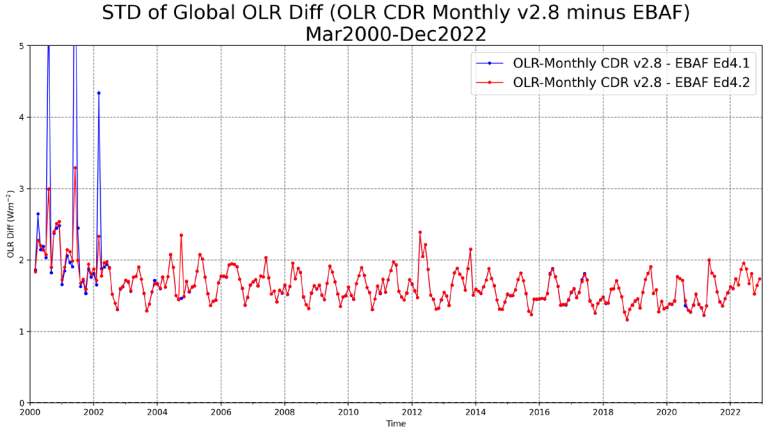

Fig. 16 Standard deviation of OLR differences for v2.8 Monthly OLR CDR relative to CERES EBAF Ed4.1 (blue) and Ed4.2 (red) products. Agreement between the Monthly OLR CDR and CERES EBAF is improved with the reprocessed EBAF data in 2000-2002 period.

References

Lee, H.-T., 2017: Outgoing Longwave Radiation – Monthly Climate Data Record Algorithm Theoretical Basis Document. CDRP-ATBD-0097 Rev 4. NCDC Climate Data Record Program

Lee, H.-T., R. G. Ellingson, and A. Gruber, 2010: Development of IASI outgoing longwave radiation algorithm. Proceedings of the 2nd IASI International Conference, Annecy, France, January 25-29, 2010.

Turner, E. C., H.-T. Lee and S. F. B. Tett, 2015: Using IASI to simulate the total spectrum of outgoing long-wave radiances, Atmos. Chem. Phys., 15, 6561-6575, doi:10.5194/acp-15-6561-2015.

IASI Level 1 Product Guide: PDF_IASI_LEVEL_1_PROD_GUIDE.pdf, EUM.EPS.SYS.SPE.990003 v9e. Dec 3, 2014.

IASI Level 1 Product Format Specification, 2011: PDF_IASI_LEVEL_1_PFS product format spec. Dec 14, 2011.

Data Quality Summary for CERES EBAF Ed4.1: CERES_EBAF_Ed4.1_DQS.pdf v.3 released 12/9/2021

Data Quality Summary for CERES EBAF Ed4.2: CERES_EBAF_Ed4.2_DQS.pdf v.0 released 12/9/2022

Data Quality Summary for CERES SYN1deg-Daily Ed4.1: CERES_SYN1deg_Ed4A_DQS.pdf 4/8/2021

References for CERES products: https://ceres.larc.nasa.gov/data/documentation/#ssf

Acknowledgment

This work is funded by the NOAA NCEI CDR program.

The IASI Level 1c data are obtained through NOAA CLASS data service.

The CrIS SDS data obtained through NESDIS STAR/UMD ESSIC data service.

These CERES EBAF data were obtained from the NASA Langley Research Center CERES ordering tool at https://ceres.larc.nasa.gov/data/.

The IASI Level 1c data reader software is modified from Eumetsat software “Generic EPS-Tools: EPS format Interactive Data Language (IDL) readers”, EPS_OO_IDL_V1_6_RELEASE.